

## Estimating Local Memory of Tropical Cyclones through MPI Anomaly Evolution

ROBERT E. HART AND RYAN N. MAUE

*Department of Meteorology, The Florida State University, Tallahassee, Florida*

MICHAEL C. WATSON

*Surflife/Wavetrack, Inc., Huntington Beach, California*

(Manuscript received 29 September 2006, in final form 24 April 2007)

### ABSTRACT

This study examines the local memory of atmospheric and oceanic changes associated with a tropical cyclone (TC). The memory is quantified through anomalous maximum potential intensity (MPI) evolution for 20 days prior to the arrival of a TC through 60 days after the TC passage. The local MPI weakens and is not restored to the evolving climatology until well after the TC has departed. Stabilization occurs through warming of the atmosphere and cooling of the ocean surface on different time scales. The time scale of MPI stabilization following TC passage is approximately 30–35 days for a tropical storm to 50–60 days for a category 3–5 hurricane, with significant storm-specific and basin-specific variability. The atmospheric stabilization (warming with respect to SST) begins with TC arrival and continues for approximately 7–10 days after passage, when the troposphere cools below normal. The rewarming of SST and the subsequent rewarming of the atmosphere occurs within approximately 35 days for all intensities, despite a positive (weakened) MPI anomaly through two months. This suggests that the atmosphere retains anomalous warmth beyond what can be attributable to sensible heating from the rewarmed SST. The maintenance of a positive MPI anomaly beyond 35 days is thus attributed to a feedback on larger scales that requires considerable further research. A TC's passage through a region does not always lead to a weakening of the MPI. In regions poleward of the sharp SST gradient, the MPI one month after TC passage is often several millibars stronger than climatology. There are also mesoscale regions of destabilization one month after TC passage that may result partially from salinity changes driven by oceanic mixing as well as changes in precipitation and evaporation.

### 1. Introduction

While recent studies have investigated climate change effects on tropical cyclone (TC) frequency and intensity (e.g., Emanuel 2005; Webster et al. 2005), comparatively few have addressed the aggregate role of TCs in modifying the large-scale climate (e.g., Sobel and Camargo 2005). TCs serve as one of the many balancing mechanisms in redistributing excess tropical heat poleward within the atmosphere through convection, eddy heat transport, and in the ocean through upwelling (Emanuel 2001; Boos et al. 2004). Indeed, previous studies argue that TCs play a seemingly significant role in the overall climate system (Newton

1972; Trenberth and Stepaniak 2003a,b), yet quantification of this aggregate role has not been fully addressed.

One step toward addressing this problem is to ask (i) how long before a TC arrives at a region does it modify the environment (atmosphere and ocean) and (ii) how long after a TC departs does that region retain “memory” of the storm’s passage? Moreover, in estimating the length of the atmosphere–ocean system memory of a TC (role in climate), there may be resulting headway toward explaining the great unanswered question in tropical meteorology of why there are approximately 80–90 TCs globally every year (Gray 1985; Frank and Young 2007). Perhaps with improved knowledge of the role of TCs within the current climate, future changes in terms of TC frequency and intensity may also be better predicted and understood.

TCs have been characterized as Carnot engines (Emanuel 1986, 1988) transporting oceanic heat to the

---

*Corresponding author address:* Robert E. Hart, Department of Meteorology, The Florida State University, Tallahassee, FL 32306.

E-mail: rhart@met.fsu.edu

colder tropopause. The extraction of heat from the tropical oceans and export to the atmosphere at higher latitudes ultimately leads to regional stabilization and cooling of the tropical oceans. However, the degree of cooling depends largely upon the depth of the oceanic mixed layer and the temperature beneath it. Indeed, considerable effort has been spent relating TC intensity change to evolving characteristics of the ocean surface and subsurface temperature and salinity structure (Elsberry et al. 1976; Black 1983; Shay et al. 1989; Robertson and Ginis 2002). Typically, the mechanical turbulent mixing caused by TC wind stresses entrains colder and saltier water from the thermocline into the oceanic mixed layer dependent upon the temperature stratification with depth (Dickey et al. 1998). As the latter layer is deepened, the SSTs cool, leaving a noticeable cold wake usually to the right of the storm track (Leipper 1967; Price 1981; Black 1983; Mao et al. 2000). If a TC lingers over its own upwelled zone or crosses that of a preceding storm, a negative feedback is typically observed and the storm weakens or fails to intensify. With the resulting cooling SST days after TC passage (baroclinic response; e.g., Mao et al. 2000), further atmospheric profile stabilization results from the concomitant reduction in interfacial energy fluxes. Conversely, it has been shown that temporally varying spatial features such as warm-core rings associated with the Loop Current in the Gulf of Mexico provided rapidly intensifying Hurricane Opal (Shay et al. 2000; Hong et al. 2000) with ample oceanic mixed-layer warmth at considerable depth, an example of a positive interfacial feedback between upwelled water and the atmosphere.

Modification of the environment by the TC is not limited to the ocean. In addition to the extensive upper-tropospheric warming produced by the TC, atmospheric subsidence associated with the secondary circulation of a TC can lead to warming of the middle-tropospheric environment well beyond the scale of the smaller cyclonic vortex. Further, there is a quasigeostrophic response of large-scale subsidence (ascent) as a TC approaches (departs) a region that modifies this large-scale heating. The accumulated tropospheric heating by a long-lived TC will lift the tropopause and may intensify subtropical ridges surrounding the TC or induce both downstream and upstream trough development (Jones et al. 2003).

Indeed, several recent case studies have highlighted significant upper-troposphere thermodynamic anomalies associated with decaying and transitioning tropical cyclones for many days afterward. For instance, Super-typhoon Dale (1996) underwent extratropical transition over the western North Pacific and rapidly translated

northward in the Arctic, propelling a warm geopotential thickness anomaly over the North Pole where it persisted for a week (Kelsey and Bosart 2006). Similarly, McTaggart-Cowan et al. (2006) demonstrated that large-scale atmospheric warm pools associated with TC remnants (e.g., Katrina) can persist and modify the global wave pattern 1–2 weeks after the TC has decayed. Likewise, Hart et al. (2007) demonstrated a correlation between the Northern Hemispheric recurring TC frequency and characteristics of the subsequent midlatitude winter climate driven by late-autumnal snow cover anomalies. Altogether, these aforementioned studies underscore the large-scale and temporally prolonged thermodynamic impacts of TCs upon their environment. Yet, before quantifying the large-scale or global impact, it is critical to quantify the regional memory of the TC.

This entire sequence of regional stabilization can be measured by maximum potential intensity (MPI), which is a theoretical maximum intensity a TC can attain given the combination of SST and atmospheric thermodynamic structure (Emanuel 1986, 1988). As the atmosphere warms and the SST cools the MPI will weaken. However, overlapping this storm-specific evolution is the MPI's climatological evolution due in part to the differing heat capacities of land versus water. Restoration of MPI to the prestorm value does not necessarily mean that the MPI anomaly is zero if MPI climatology has changed. Thus, any stabilization caused by the passage of a TC should be measured with respect to the evolving climatological mean MPI for that location.

This study, an extension of Watson (2005) in time and space, seeks to quantify the memory of a TC through the region it tracked. While Watson (2005) examined the impact of using a mixed-layer depth of climatological-mean ocean temperature as input into the MPI calculation for pre- and poststorm evolution, this study uses the daily SST to describe the oceanic evolution. Watson (2005) examined the MPI memory of a TC's passage but ignored the evolving climatological MPI evolution in the memory calculation. Here, a daily climatology of MPI is calculated and the evolution of storm-environment MPI with respect to this climatology is then calculated for every North Atlantic (NATL), eastern North Pacific (EPAC), and western North Pacific (WPAC) TC until landfall from January 1985 to August 2002. In short, the goal of this study is to quantify the oceanic (SST) and atmospheric memory of TCs. The data and method used are explained in section 2, results are given in section 3, conclusions in section 4, and discussion in section 5.

## 2. Data and method

### a. Data

Tropical cyclone track data are from the National Hurricane Center (NHC) best-track dataset (Jarvinen et al. 1984; Neumann et al. 1993) and the Joint Typhoon Warning Center (JTWC) best-track dataset (Chu et al. 2002). The tracks used incorporate the NATL, EPAC, and WPAC basins. North Indian Ocean (NIND) TCs are excluded largely because of a greater degree of uncertainty in their track and intensity (e.g., Landsea et al. 2006) as well as the considerably shorter life span.

The atmosphere is represented here by approximately  $1.125^\circ \times 1.125^\circ$  grids spaced 6-h 40-yr European Centre for Medium-Range Weather Forecasts (ECMWF) Re-Analysis (ERA-40; Uppala et al. 2005) of sea level pressure (SLP), temperature, and moisture from 1985 to August 2002. Although the size and intensity of ERA-40 representation of the TC's inner-core structure is greatly underestimated (Manning and Hart 2007), the anticyclonic structure aloft is better resolved given its larger-scale and weaker gradients (Frank 1977). Nevertheless, the results found here are specific to the datasets used. Complementary results (not shown) demonstrate that shifting to a coarser atmospheric dataset [e.g., National Centers for Environmental Prediction–National Center for Atmospheric Research (NCEP–NCAR) reanalysis; Kalnay et al. 1996] does not significantly change the length of stabilization periods but does change the amplitude of the stabilization for the few days when the TC is nearby.

The SST in this analysis is represented by the National Aeronautics and Space Administration (NASA) optimal interpolation (OI)  $\frac{1}{4}^\circ$  daily averaged dataset (Reynolds et al. 2006; acquired from <ftp://eclipse.ncdc.noaa.gov/pub/OI-daily/>). As this dataset is a daily average, the issue of longer temporal averaging associated with other datasets (e.g., Reynolds weekly averaged) is reduced. In particular, this lessens the concern that temporal smoothing of the SST could lead to mixing of SST representation across the “before storm” and “after storm” boundary, which is essential to the goals of this analysis. Nevertheless, there may be some temporal bleeding across this boundary when the TC cloud cover canopy prevents the local SST from being observed remotely by microwave frequency satellites. Consequently, it is expected that at least a day of temporal smoothing is inherently present in the analyses presented here.

For atmospheric temperature, moisture, and SLP, a 6-hourly 17-yr climatology of the ERA-40 dataset (1985–2001) was produced for every grid point. A corresponding daily 17-yr climatology of the SST dataset

was produced for every grid point. The resulting climatology combination of atmosphere and SST provides a climatological MPI control dataset to compare against the storm-specific MPI evolution. Ideally, one would desire an MPI climatology of at least 30 yr. However, the dataset lengths used here preclude that. Consequently, the MPI climatology here is prone to bias toward the higher recent frequency of warm ENSO phases.

### b. Method

The integrated atmospheric and oceanic surface stabilization by TCs is measured using MPI (Emanuel 1988). This calculation utilizes the atmospheric profile of temperature, moisture, SLP, and SST to estimate the maximum TC intensity that atmospheric/oceanic profile can produce assuming a Carnot cycle approximation to TC energetics. The areal-average SST and atmospheric profile of temperature, moisture, and SLP over a TC-centered  $5^\circ \times 5^\circ$  box (e.g., Fig. 1a) were input to the Emanuel (2006) MPI routine described by Emanuel (1988). Given the grid spacing of the various datasets involved, approximately 16 ERA-40 grid points and 400 SST grid points were utilized in the area average of the  $5^\circ \times 5^\circ$  box. Holding the location of the box fixed, this MPI calculation was performed for evolving atmosphere and SST 20 days prior to storm arrival in the fixed box through 60 days after storm arrival (e.g., Fig. 1b, solid line). Thus, for every 6-h best-track storm location there are 81 values of MPI. With over 32 000 storm locations in this analysis (Table 1), there are approximately 2.6 million MPI values composing the analysis here (1.5 million for tropical storm intensity or greater). The storm database was limited to those storm locations equatorward of  $35^\circ\text{N}$  to focus on stabilization resulting predominantly from the TC itself rather than interacting midlatitude features. All stages of the best-track TC life cycle were included (tropical depression through hurricane/typhoon, as well as subtropical and extratropical), as long as the storm location was equatorward of  $35^\circ\text{N}$ . The subtropical and extratropical phases together make up approximately 0.5% of the total analysis.

This process was then repeated using the 17-yr average climatological atmospheric and SST conditions to determine a climatological MPI time series for the same 20 days prior to storm arrival through 60 days after storm arrival (e.g., Fig. 1b, dotted line). Subtraction of these produces a time series of MPI anomaly (e.g., Fig. 1b, bar chart). As the TC approaches, passes through, and departs the box, the atmospheric temperature profile (e.g., Fig. 2b) will change with respect to the ocean (e.g., Fig. 2a) leading to convective stabilization or de-

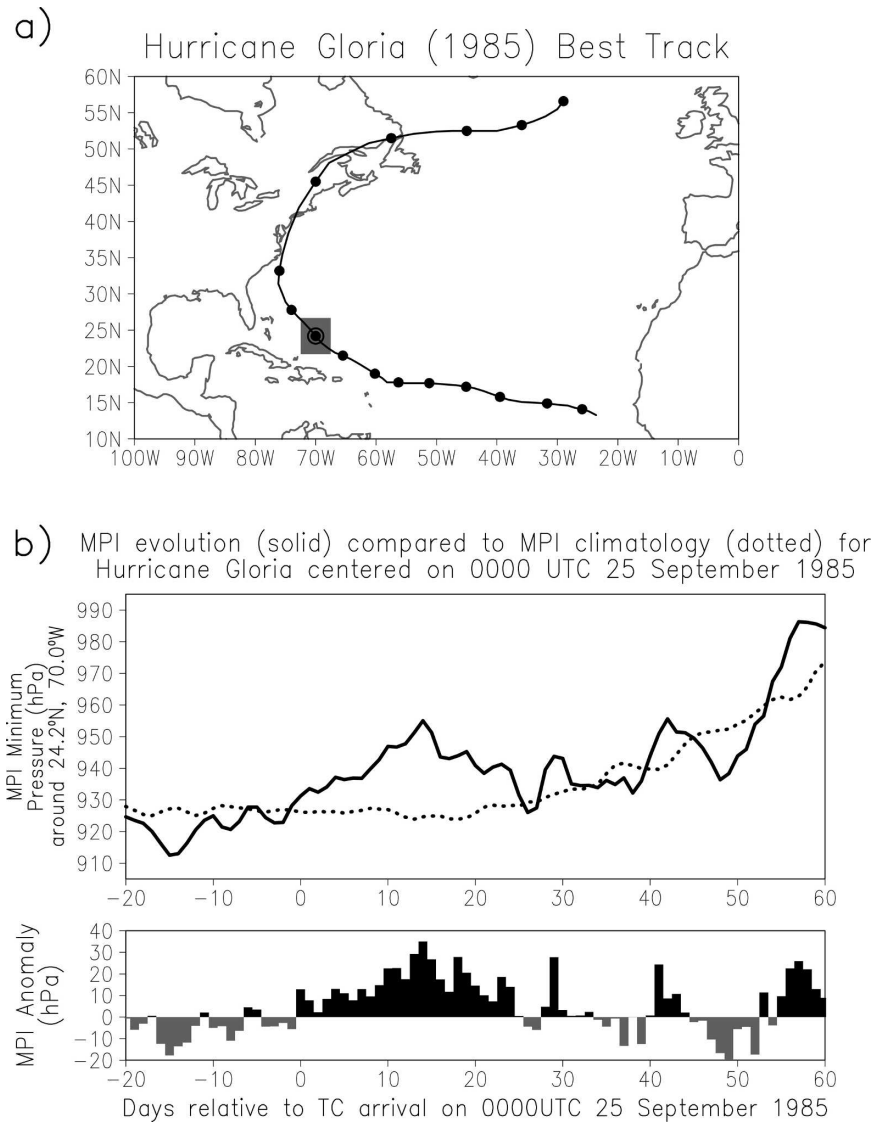


FIG. 1. Example of the temporal evolution of MPI anomaly for Hurricane Gloria (1985) relative to its location at 0000 UTC 25 Sep 1985. (a) NHC best track for Gloria, with the position at 0000 UTC 25 Sep 1985 labeled by the circle at the center of the gray box. The 0000 UTC positions at days prior to and after this date are given by the solid circles. The gray box is the  $5^{\circ}$  latitude  $\times$   $5^{\circ}$  longitude box over which the areal mean atmospheric and sea surface temperature values are calculated using the datasets described in the text. The position of that box does not change in time for each of the 81 (20 days prior through 60 days after TC passage) MPI calculations shown here. (b) Plot of MPI (solid) within the gray box in (a) and of climatological MPI for that box (dotted). The bar chart is the MPI anomaly, the subtraction of the two time series in the panel above.

stabilization. This method effectively tracks the magnitude of this stabilization or destabilization. Other mesoscale or synoptic-scale features (atmospheric and oceanic) may pass through the box well before or after the TC arrives. An example of this would be beyond 30 days after TC arrival in Fig. 1b. Given the increasing magnitude of the MPI anomaly cycle beyond 30 days in Fig. 1b it is reasonable to assume that other TCs (e.g.,

Hurricane Kate of 1985) or midlatitude troughs are dominating the fluctuations shown at that time rather than residual effects from the long-departed Hurricane Gloria. Consequently, the results found here should be viewed in the context of an evolving atmosphere and ocean that may or may not be entirely as a result of the TC. Examples of time series of two other storms are shown in Figs. 3a,b and will be discussed at length later.

TABLE 1. Average age (h) of a TC as a function of basin and instantaneous intensity. The first row of numbers in each cell is the average age and the standard deviation separated by a slash. The second row of numbers in each cell is the number of cases. Source for this analysis is the official best-track dataset for each respective basin for the period 1985–August 2002, limited to those storm locations within 35° of the equator. The padding between the cells represents statistical significance between adjacent cells: 90% (light gray), 95% (dark gray), and 99% (black) significance through a Student's *t* test. The NATL column is repeated to permit *t*-test comparison with WPAC. The first record in the best-track dataset for a given storm represents the zero hour in the age. It should be noted that the criteria for starting and ending points for life cycle vary among the basins and thus do not necessarily represent the entire life cycle of the TC. The final row in the table represents the average age of the TC at the last advisory in the best-track dataset (the lifespan of the average TC), not limiting the occurrence latitudinally.

Stage	NATL	EPAC	WPAC	NATL	ALL
Tropical depression	68.4 / 75.6 (1331)	101.1 / 100.2 (2662)	77.2 / 79.9 (8787)	68.4 / 75.6 (1331)	81.3 / 84.8 (12780)
Tropical storm	85.9 / 69.1 (1871)	93.1 / 89.7 (3117)	137.3 / 87.8 (5254)	85.9 / 69.1 (1871)	114.4 / 88.6 (10242)
Category 1	120.8 / 64.4 (783)	123.5 / 84.6 (1108)	168.1 / 84.5 (2253)	120.8 / 64.4 (783)	147.3 / 84.2 (4144)
Category 2	144.0 / 71.4 (291)	133.3 / 81.8 (595)	182.0 / 79.1 (1181)	144.0 / 71.4 (291)	162.6 / 82.0 (2067)
Category 3	160.8 / 67.4 (178)	132.6 / 81.3 (412)	185.3 / 75.4 (655)	160.8 / 67.4 (178)	164.3 / 79.9 (1245)
Category 4	161.9 / 52.0 (163)	140.8 / 94.4 (342)	195.2 / 76.5 (825)	161.9 / 52.0 (163)	177.1 / 82.6 (1330)
Category 5	132.4 / 16.9 (14)	258.2 / 143.8 (39)	210.3 / 86.9 (227)	132.4 / 16.9 (14)	213.1 / 97.8 (280)
Total age (last record in best track)	185.7 / 106.2 (190)	165.0 / 96.8 (290)	203.2 / 101.8 (571)	185.7 / 106.2 (190)	189.5 / 102.5 (1051)

This stabilization calculation (20 days prior to storm arrival through 60 days after departure) was performed for every 6-h storm location over water for all NATL, EPAC, and WPAC storms from January 1985 to August 2002. The number of storm locations as a function of basin and intensity is given in Table 1. The results of this MPI anomaly analysis as a function of storm intensity and basin are presented next. All MPI anomalies are represented with respect to minimum SLP. Thus, a positive MPI anomaly represents weakening (stabilization) with respect to climatology.

### 3. Results

#### a. Total MPI evolution

The mean MPI anomaly for all NATL, EPAC, and WPAC storms from 20 days prior to arrival to 60 days after arrival is shown in Fig. 4. Positive values of MPI anomaly represent stabilization and warming of the atmospheric column with respect to the SST. Two to three weeks before a storm approaches a region, the MPI anomaly is largely constant—varying within a 1–2-mb range. Interestingly, the magnitude of this anomaly (+1 to +3 mb) argues that TCs generally move into an atmosphere (SST) that is slightly warmer (cooler) than climatology (Fig. 5a) consistent with Evans (1993) and possibly explained in part by Ramanathan and Collins (1991). The positive MPI anomaly amplifies approximately 4–5 days prior to the storm's arrival. This weakening is a consequence of the larger-scale upper-

atmospheric warming from the TC (Fig. 5b) overwhelming the warming of the SST (Fig. 5a). Depending upon translation speed of the TC, increasing cirrus one to two days prior to TC arrival may also further weaken MPI through increased albedo (Ramanathan and Collins 1991; Sobel and Camargo 2005). The relative oceanic versus atmospheric proportions of these MPI changes are again implied by Fig. 5 and examined in more detail in section 3b.

By the time of the storm's arrival in the box, the MPI is 5–10 mb weaker than climatology, and this positive MPI pressure anomaly continues to grow after the storm departs. The peak stabilization appears to be 4–5 days after TC passage consistent with numerical simulations of poststorm oceanic baroclinic response (Mao et al. 2000). Thereafter, the positive MPI anomaly slowly weakens as the ocean rewarms (Fig. 5a) and the atmosphere rapidly cools (Fig. 5b) with the departure of the TC. The average time it takes the MPI to return to climatology (time varying) ranges from approximately 35 days for a tropical storm to approximately 2 months for a major hurricane. Significant case-to-case variability in this memory is noted and illustrated by Figs. 1 and 3a,b. The length of regional memory of a TC implies that the aggregate impact of TC warming of the atmosphere and cooling of the upper ocean is long-lived and can extend well into the autumn.

This restoration of MPI to climatology appears to result from a combination of factors. First, the cooling of the ocean with respect to the atmosphere (Fig. 5a

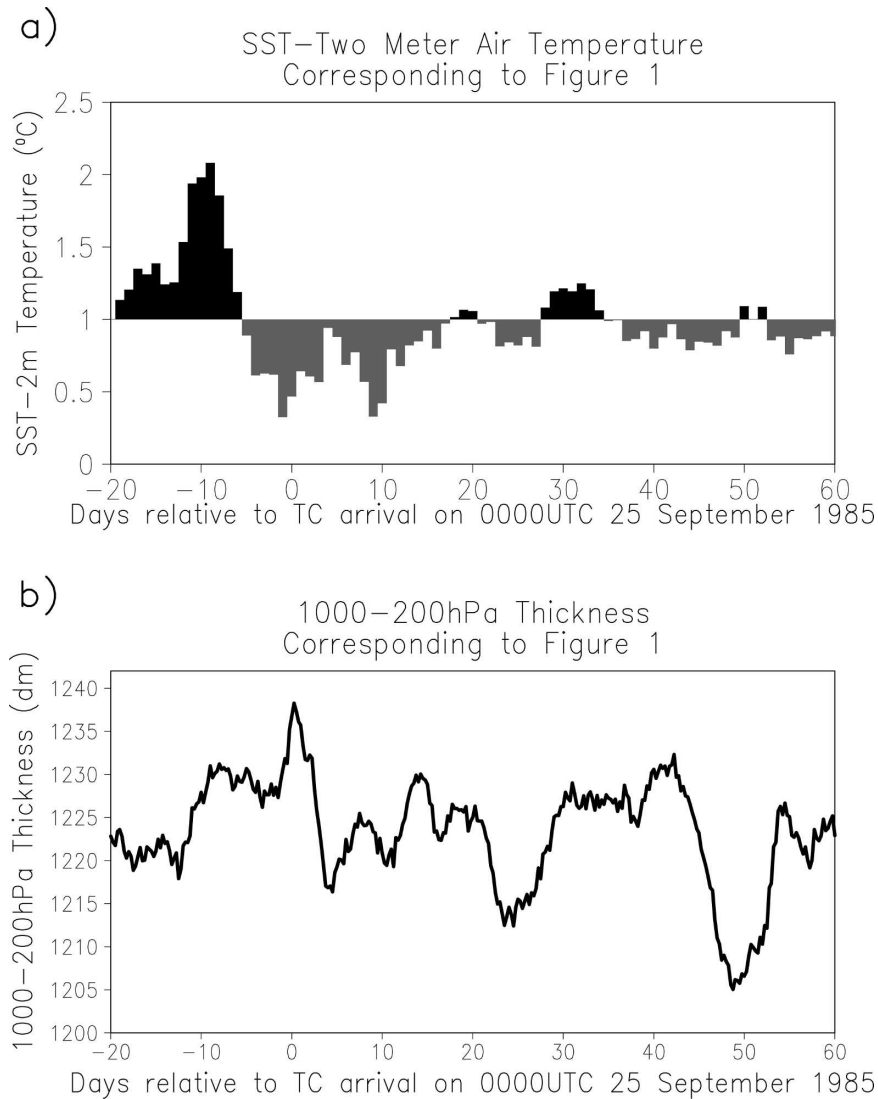


FIG. 2. (a) Difference between SST and 2-m air temperature ( $^{\circ}\text{C}$ ) in the box defined by Fig. 1a, for 20 days prior to 60 days after the passage of Hurricane Gloria (as in Fig. 1). (b) Same as in (a) but for 1000–200-hPa thickness.

versus Fig. 5b) results in a weakening of the upward heat flux (e.g., Fig. 2a). Second, the stabilization of the column with respect to convection (implied by Fig. 2) would lead to an increase in short-wave insolation at the ocean surface, given the concomitant anomalous low cloud cover. Finally, in many cases after the strongest climatological MPI (Fig. 6a), the evolving climatological MPI weakens and “catches up” to the slowly strengthening MPI within the box. The NATL climatological MPI begins weakening in late September through October (e.g., Figs. 1b, 3, 6) such that the actual MPI anomaly may return to zero even if the absolute MPI itself is not strengthening. This effect is least significant in the first third of the season (e.g., Fig. 3a)

and becomes increasingly significant in the latter third of the season (e.g., Fig. 3b). This date of the peak climatological MPI also varies regionally (Fig. 6a), and may also differ significantly from the date of peak TC occurrence (Figs. 6b,c). From Fig. 6c, one can conclude that in the majority of the NATL and EPAC the evolving MPI climatology delays the restoration of memory while in the extreme western WPAC it is accelerated.

It is interesting that the peak climatological MPI occurs well after the TC season peak in the EPAC and NATL, but considerably before the TC season peak in WPAC (Fig. 6c). Explaining definitively the causes for this is worthy of further study. Overall, one would expect the peak MPI to occur in the autumn rather than

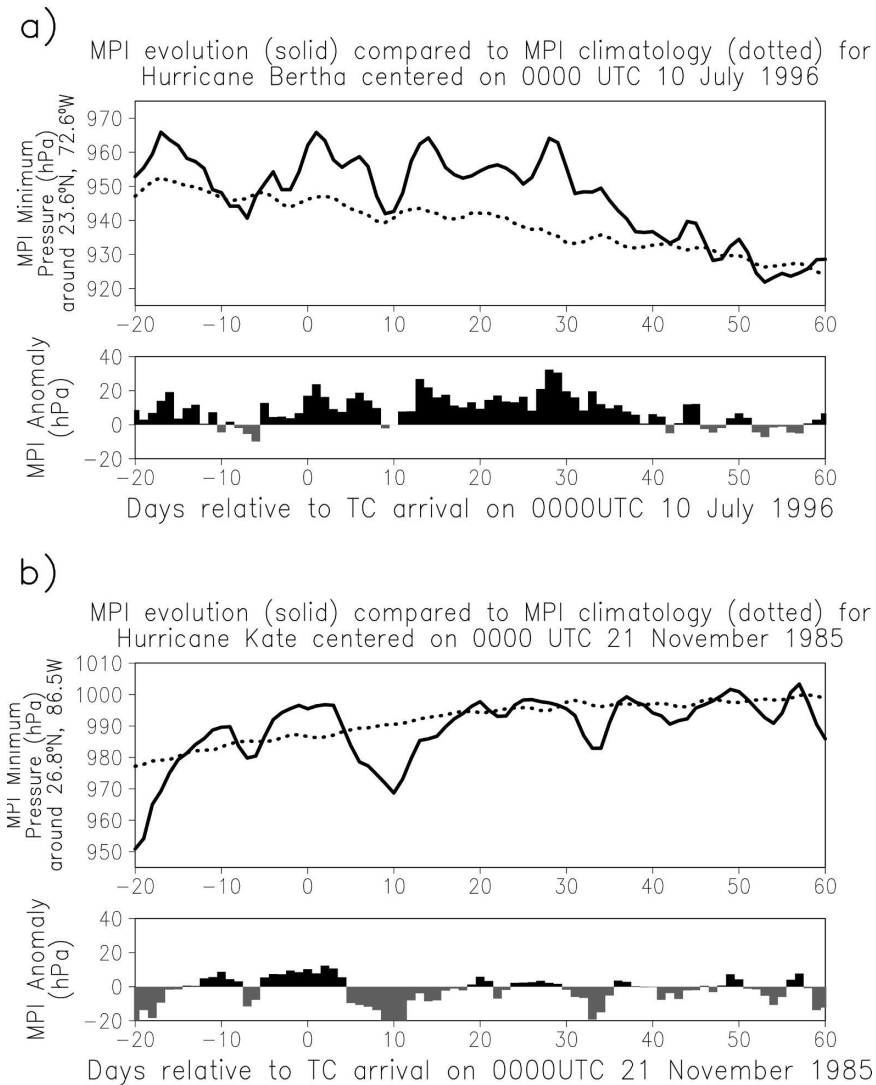


FIG. 3. As in Fig. 1b, but for two Atlantic TCs during the beginning and end of the TC season. (a) Hurricane Bertha (1996) during July, after which the MPI restored to climatology almost two months later. (b) Hurricane Kate (1985) during November, after which the MPI restored to climatology within a week. It is worthwhile noting that these two storms occurred in different parts of the basin. Yet a month after Bertha (1996) other Atlantic TCs passed nearby Bertha's prior track. Consequently, the varying restoration time scales shown are more than a function of month of occurrence. Further note that Kate (1985) occurred in a different location than Gloria (1985; Fig. 1), yet may have overlapped in track for a period of time.

summer since the atmosphere cools faster than the SST as a result of differing heat capacities and the increasing prevalence of midlatitude troughs; the net result is larger convective available potential energy (CAPE) and more intense MPI. While this may be the case in the EPAC and NATL, clearly it is not in the WPAC. In the EPAC and NATL, TCs have lower annual counts (and are smaller overall) than in the WPAC (Elsberry 1995). Thus, upwelling from TCs (and a decrease in MPI) contribute less to the climatology of MPI in the EPAC and NATL than in the WPAC. In the WPAC,

TCs are a more dominant contributor to the MPI climatology itself. Thus, the peak MPI occurs before WPAC TCs rapidly increase in number in July (Elsberry 1995). It is also possible that the seasonal cycle of the monsoon trough in the WPAC causes the peak climatological MPI to occur earlier in the summer than in the other two basins—through changes in both the atmospheric sounding and the wind-stress-induced upwelling. Moreover, since there is a bias toward positive ENSO events in the period of record used, it is also possible that the typical seasonal cycle of ENSO—and

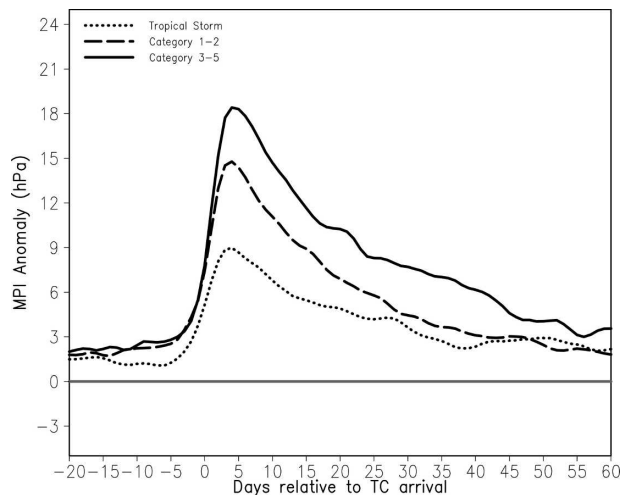


FIG. 4. The evolution of MPI anomaly for all Northern Hemisphere storms equatorward of  $35^{\circ}\text{N}$  from 1985 through 2002: tropical storms (dotted), category 1 and 2 tropical cyclones (dashed), and major tropical cyclones (category 3 or higher; solid). MPI anomaly is relative to the 17-yr mean from 1985 through 2001. Abscissa is days relative to the arrival of a TC in a fixed box of  $5^{\circ} \times 5^{\circ}$  size (see text). The intensity (tropical storm, category 1 or 2 hurricane, major tropical cyclone) is based upon the intensity at the time it arrives in the “box,” at time “0” on the abscissa.

its associated SST anomalies—is also driving the earlier MPI peak in the WPAC compared to the other two basins. Regardless of the causes, as stated earlier, the phase shift shown in Fig. 6c argues that the cycle of peak MPI causes an extension of memory in the EPAC and NATL and a truncation of it in the WPAC.

The stabilization period is clearly a function of intensity as mentioned earlier and appears to be partly due to the aggregate effects from the storm’s history. Stronger storms are more likely to have existed for a longer period of time (Table 1) producing a larger area of anomalously cool SST and anomalously warm tropical atmosphere (Fig. 5), both of which advect at considerably slower speeds than the translation of the cyclonic atmospheric vortex itself. Stronger storms also produce greater upwelling (Fig. 5a) that may extend the local memory of the TC.

The basin-specific response of TC stabilization is shown in Fig. 7. The NATL and WPAC share similar profiles of stabilization although the EPAC differs considerably. The EPAC has a less amplified stabilization and shorter time scale (by approximately half on both measures). This truncated memory may be partly a consequence of the shorter lifespan of EPAC TCs (Table 1) due to a smaller areal coverage of warm SSTs and a very sharp meridional SST gradient. Moreover, the vertical profile of oceanic temperature in the EPAC is considerably more stratified near the base of the mixed

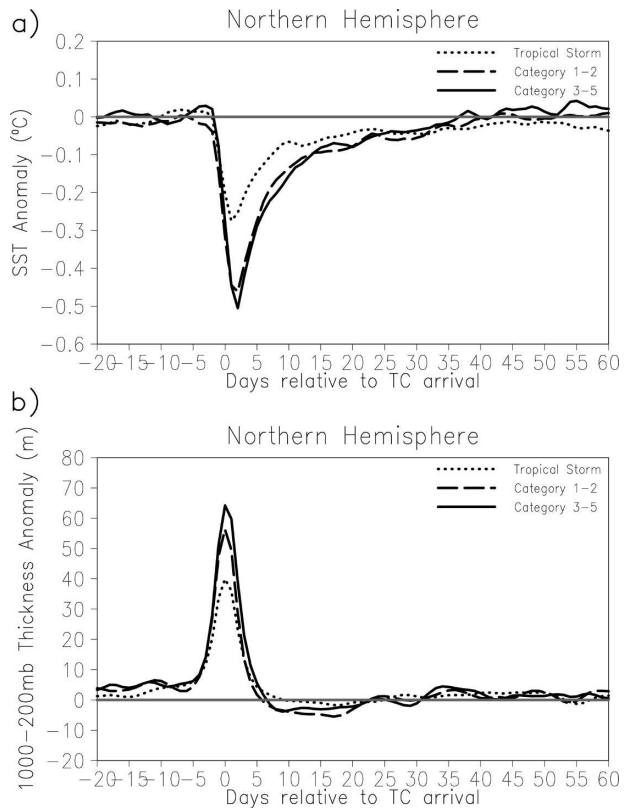


FIG. 5. (a) SST anomaly (from 17-yr daily mean) and (b) 1000–200-hPa thickness anomaly (m) from 17-yr 6-h mean corresponding to Fig. 4.

layer (Brewster and Shay 2006) leading to a reduction in the magnitude of upwelling by TCs (e.g., Subrahmanyam et al. 2005). This is supported by Fig. 7b given that there is little difference in memory or amplitude of stabilization among the two hurricane subsets. The smaller size of EPAC TCs compared to NATL and WPAC might also contribute to the truncated memory.

There appears to be a wave nature to the restoration of MPI after storm arrival in all three basins, although it is much more apparent in the NATL basin. The potential source of these waves and whether these waves change the MPI through primarily oceanic changes or atmospheric changes will be addressed next.

#### b. Atmospheric and oceanic contributions to MPI changes

The contribution of the atmospheric changes to the total MPI anomaly in Fig. 4 is assessed by fixing the SST to daily climatology and repeating the MPI anomaly calculations performed earlier. It should be noted that the atmosphere in this second analysis is not evolving independently of the SST. Even though the SST is fixed to the evolving daily climatology in this second analysis, the lower atmosphere is not insulated from (and is re-

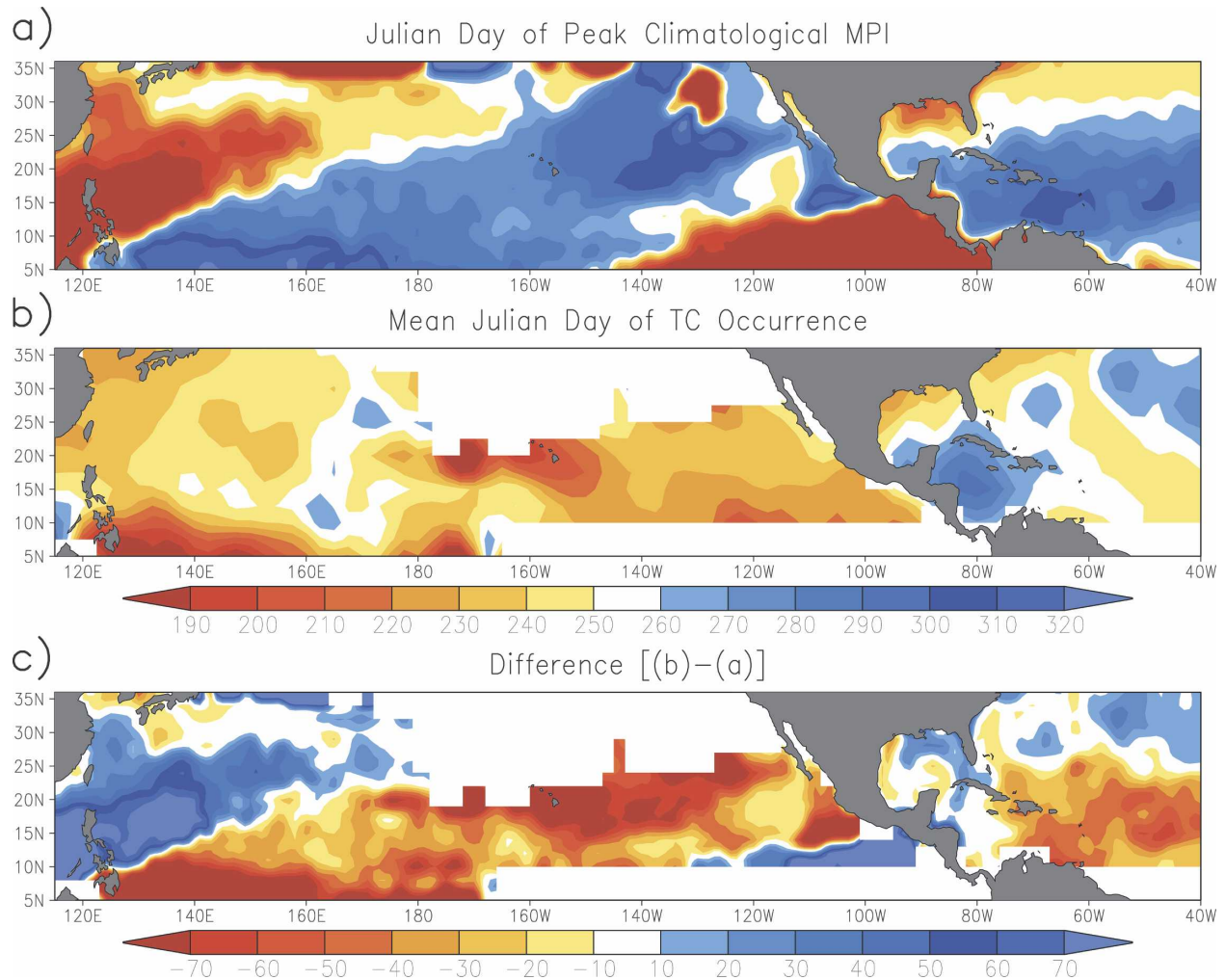


FIG. 6. (a) Julian day of peak climatological MPI, (b) mean Julian day of TC occurrence for the storms utilized here, and (c) difference between (b) and (a). Negative (positive) values in (c) indicate that TCs occur after (before) the peak climatological MPI on average. For reference, 10 Sep, the climatological peak occurrence of NATL TCs, is Julian day 253.

sponding to) the actual changing SST. Thus, this analysis is only approximating the atmospheric component to the evolving MPI anomaly and will be referred to as the pseudoatmospheric MPI (PAMPI).

The positive PAMPI anomaly (Fig. 8a) weakens in the five days leading up to storm arrival through a combination of potential destabilizing factors. As the TC approaches the box, lowering SLP within the box along with a drying from large-scale subsidence may overcome the upper-tropospheric warming (e.g., Fig. 5b) in the MPI calculation. This subsidence is further increased by the quasigeostrophic response to decreasing cyclonic vorticity advection with height prior to TC arrival, although may be mitigated by the quasigeostrophic response to warm advection associated with the TC. Further, the actual evolving SST a few days before TC arrival (e.g., Fig. 5a) is likely driving lower-

tropospheric temperature changes that cannot be accounted for by the fixed climatological SST used. For the early stages of TC development, the stabilization prior to storm arrival may also result from large-scale preconditioning: monsoon trough changes (Harr and Elsberry 1995a,b), intertropical convergence zone (ITCZ) breakdown (Hack et al. 1989; Schubert et al. 1991), Saharan dust-layer modulation (Carlson and Prospero 1972; Karyampudi and Pierce 2002), and a host of other large-scale changes (Briegel and Frank 1997; Sobel and Camargo 2005).

Once the storm passes, the positive PAMPI anomaly increases by a few millibars. This atmospheric stabilization is a consequence of the broad mid- and upper-tropospheric warmth associated with the TC (Fig. 5b) and its associated anticyclone along with rising SLP. There is also likely a significant component of lower-

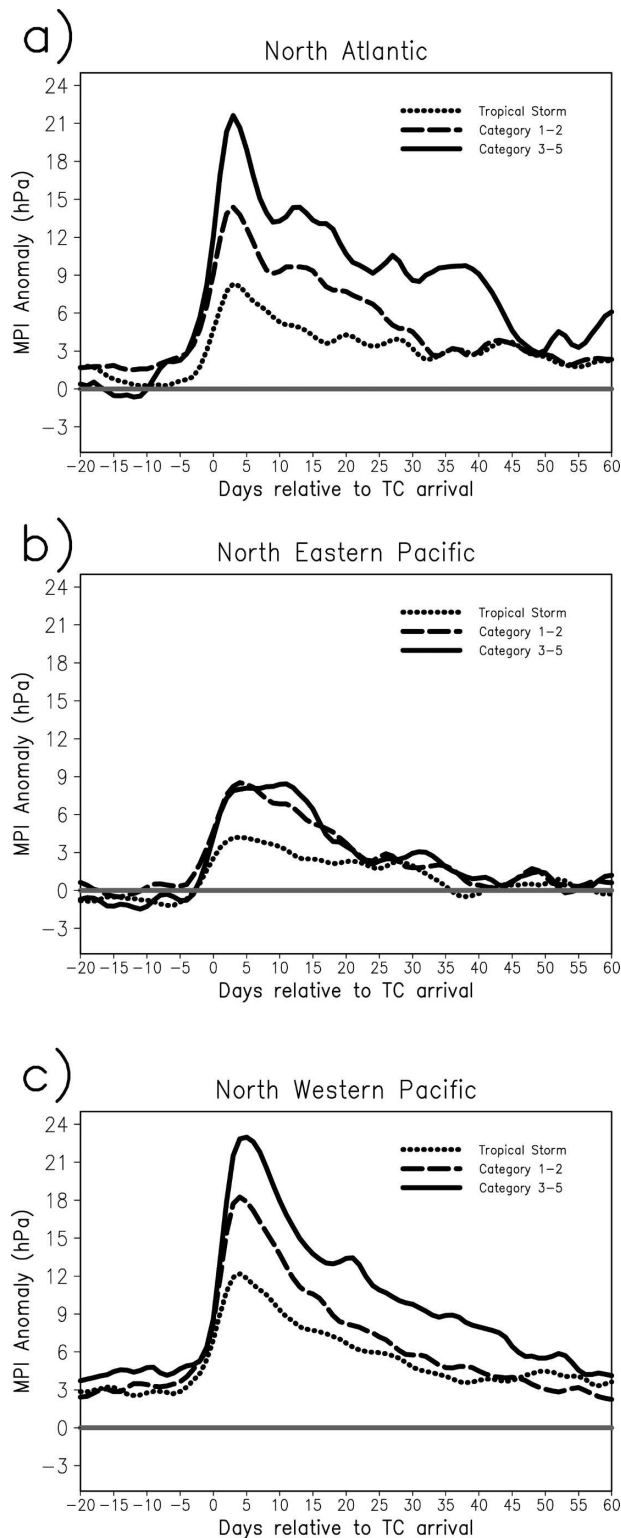


FIG. 7. As in Fig. 4, but for the individual basins: (a) North Atlantic, (b) eastern North Pacific, and (c) western North Pacific. The basin-frequency weighted mean of the three above produce Fig. 4.

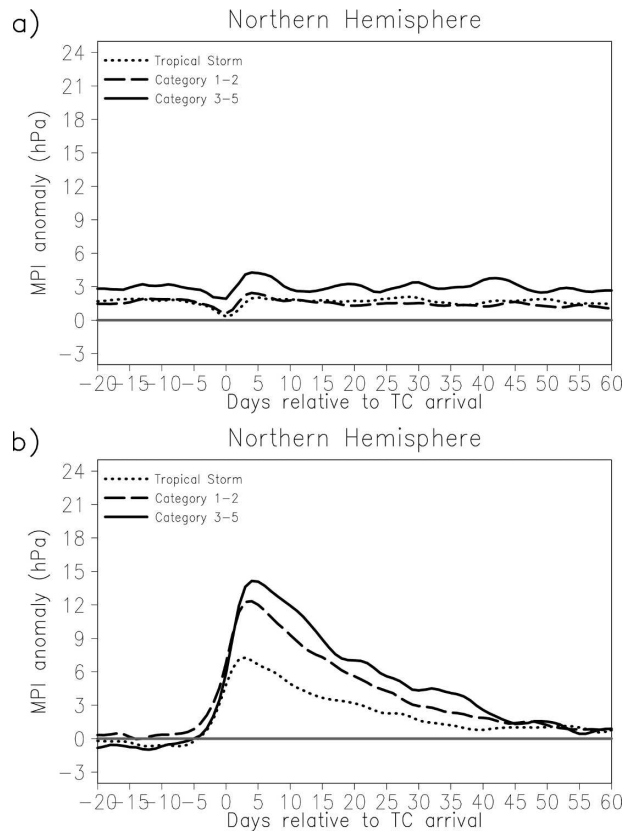


FIG. 8. As in Fig. 4, but keeping (a) SST fixed to the daily climatological value. Thus, the MPI anomaly shown in (a) is a function of the evolving atmosphere (ERA-40) within the box. (b) The total MPI anomaly in Fig. 4 minus the curves in (a); hence, the estimated oceanic contribution to the total MPI anomaly.

atmospheric cooling from the actual cooling SST (Fig. 5a). The PAMPI anomaly returns to prestorm values approximately 7–10 days after storm passage, suggesting that the tropical atmospheric memory of a TC has a length of approximately a week, consistent with Fig. 5b. However, as Figs. 5a and 7b suggest and from earlier discussion, the oceanic memory of a TC is much longer.

Comparing Fig. 8a to Fig. 8b it is evident that the pseudoatmospheric component of the total MPI anomaly is approximately 15%–20% of the total and has a stronger wave nature than the oceanic component. The wave nature of Fig. 8a is also present in Fig. 5b, made more apparent in the zoomed-in Fig. 9, and has a period of approximately 1–2 weeks. Although the amplitude of the waves is a maximum in the NATL basin, it is present in all three basins (Figs. 9a–c). Since the amplitude of the waves is greatest in the Atlantic basin and decreases westward, there is some evidence that the waves themselves are potentially tropical easterly waves. Yet the documented period of tropical easterly waves of about 3–5 days (Burpee 1972) suggests

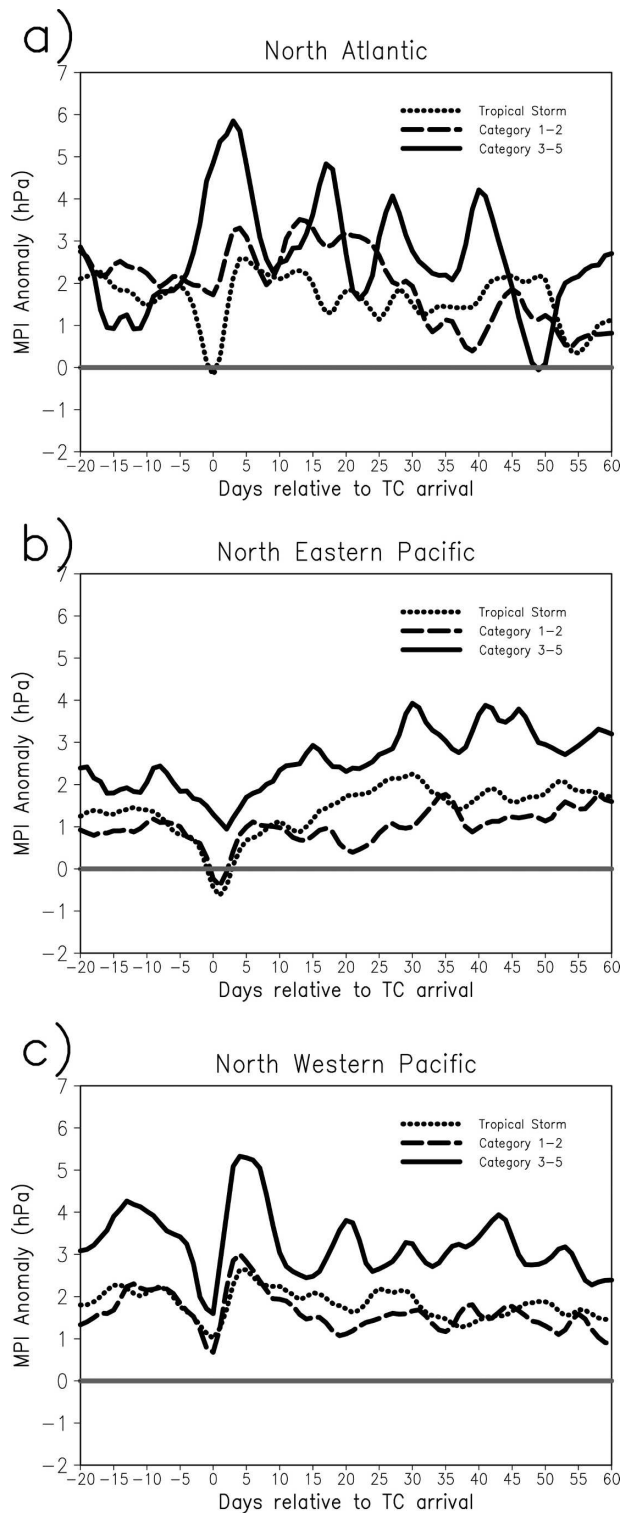


FIG. 9. A close-up of Fig. 8a for the (a) North Atlantic basin, (b) eastern Pacific basin, and (c) western North Pacific basin. Note the scale has changed from prior figures.

that the waves shown in Fig. 9 likely have another (or additional) source. Recent research has demonstrated that there are numerous tropical atmospheric wave types that contribute to tropical cyclogenesis (Wheeler and Kiladis 1999; Roundy and Frank 2004; Frank and Roundy 2006). The longer period of waves in Fig. 9 may result from a phasing of the 3–5-day period for tropical easterly waves with waves of longer periods (e.g., mixed Rossby–gravity waves, equatorial Rossby waves, and the Madden–Julian oscillation; Frank and Roundy 2006). Indeed, in the context of Frank and Roundy (2006) the 1–2-week periodicity shown in Fig. 9 might be MPI modulation driven by phasing of equatorial Rossby waves and mixed Rossby–gravity waves.

When focusing on the wave nature for MPI anomaly associated with major TCs (Fig. 9), it is curious that the wave nature extends backward in time in the EPAC and WPAC, but less so for the NATL. This difference may in part explain the source of the waves (geographically) in relation to the varying basins. It is additionally curious that the amplitude of the atmospheric waves of MPI is so much stronger for major TCs. However, it may be that the major TC occurrence is simply acting as a geographic or temporal proxy for regions/months that are more conducive for these waves. Conversely, perhaps major TCs themselves act to trigger other wave types (e.g., Jones et al. 2003) that then modulate the MPI field as they propagate within and outside the tropics.

Last, it should be noted that the wave structure shown in Fig. 9 may in part be a synthetic result of forcing the PAMPI calculation to occur using an evolving atmosphere and climatological SST that are not in balance. However, the existence of waves in Fig. 5 (Fig. 5b, in particular) argues that imbalance plays a small role on the production of waves. Further research into the source of the waves within Fig. 9 is necessitated but beyond the scope of this paper.

### c. The paradox of oceanic versus atmospheric memory

When comparing Fig. 4 to Fig. 5 we are presented with an interesting paradox. As stated earlier, the memory of the TC is approximately 1–2 months as measured by MPI anomaly (Fig. 4). It has been argued that the atmospheric component to this lasts approximately a week, and the remainder of the memory results from the cooled SST (Fig. 8). Yet Fig. 5 argues the situation is considerably more complex than this. The TC memory as calculated by SST anomaly appears to be approximately 35–40 days regardless of TC intensity (Fig. 5a). Thus, the extension of MPI memory beyond 35–40 days for hurricanes cannot be explained solely by SST changes. Although SST returns to climatology approximately 40 days after TC departure (Fig. 5a), the

mean tropospheric virtual temperature (thickness; Fig. 5b) actually goes above normal 30 days after TC departure. Further, it appears that the warming/moistening of the troposphere is beyond that accounted for by the SST warming (Fig. 5a), since the resultant MPI anomaly (Fig. 4) is significantly positive (weaker than climatology) beyond 35 days. This implies that there may be a sustained (net) warming of the tropical atmosphere that results from TC occurrence, possibly representing a nonlinear feedback. In short, the aggregate memory of a TC locally may be more than the sum of the memory of the SST and atmospheric measures separately. This argues that the net impact of a TC on the tropics is net atmospheric stabilization with respect to the SST.

Conversely, it must also be noted that this paradox may be explained by larger-scale factors (e.g., ENSO) that are known to modulate TC occurrence regionally. The sustained MPI anomaly beyond 35 days through two months for major hurricanes may in part be related to large-scale changes induced by ENSO that also shift the location and intensity of TC occurrence. Clearly the cause of this apparent paradox needs substantial additional investigation to determine how much of the excess memory can be attributed to nonlinear feedback of the TC itself versus large-scale forcing.

#### d. Intrabasin variability in atmospheric/oceanic memory

The variability among the basins shown in Fig. 7 suggests that the structure of the upper ocean plays a significant role in the length of memory of TCs. To further examine this relationship the mean MPI anomaly 30 days after TC passage is calculated as a function of location (Fig. 10a). Immediately apparent is that there is considerable intrabasin variability of TC memory. Those regions with the greatest potential for upwelling appear to retain the largest positive (weakened) MPI anomaly after 30 days. However, there are also areas of the basins that exhibit negative MPI anomalies 30 days after TC passage. In these regions—which appear to partially coincide with regions with SST < 26.5°C (black line in Fig. 10a)—the MPI is actually more intense than climatology 30 days after TC passage. Explaining this intensified MPI is not as straightforward and would benefit from further examination with both observations and coupled modeling. In their absence, potential explanations for this relationship based upon prior research include the following:

- (i) The weakening TC in these regions leads to a temporary downward heat flux (into the sea surface) with the warmer-than-normal atmosphere warm-

ing the cooler-than-normal SST (e.g., Black and Holland 1995).

- (ii) Wind stress caused by the TC may lead to slow horizontal advection of the slightly warmer oceanic mixed layer poleward over the cooler SST (e.g., Black et al. 1988).
- (iii) The days to weeks during a TC's formation and intensification leads to the development of an anomalously strong upper-troposphere anticyclone that often remains in the subtropics after the low-level cyclone is destroyed or advected poleward (e.g., McTaggart-Cowan et al. 2006; Hart et al. 2007). This residual anticyclone would further stabilize the subtropical environment (e.g., Fig. 5b), leading to enhanced insolation (e.g., Sobel and Camargo 2005), enhanced warming of the subtropical SST, and above-normal MPI.
- (iv) The profile of cyclonic (anticyclonic) vorticity advection weakening with height ahead (behind) the TC leads to a quasigeostrophic response of large-scale subsidence (ascent). The profile of temperature advection associated with the TC leads to a vertical motion response that mitigates the differential vorticity advection-induced vertical motion couplet. This induced large-scale circulation may modulate (iii) in the week prior to and after TC passage.
- (v) Voluminous rainfall from the decaying TCs in the subtropics may lead to a lens of low-salinity water on top of the upwelled high-salinity SST (e.g., Hong et al. 2000), which would inhibit further upwelling, reduce overall mixing (Robertson and Ginis 2002; Jacob and Koblinsky 2007), increase SST (Field 2007), and strengthen MPI.
- (vi) Recurring tropical cyclones often produce strong warm air advection ahead and cold air advection behind, often significantly modifying the vertical heat flux pattern days after TC passage.
- (vii) Finally, it should not necessarily be expected that the prestorm MPI anomaly is zero. Indeed, as shown in Fig. 4, the prestorm MPI anomaly averages from +1 to +2 hPa and may have considerable intrabasin variability as well. Thus, the result shown in Fig. 6 may be a combination of sustained large-scale anomalies from the prestorm environment (e.g., ENSO) along with the TC impacts themselves. It is reasonable to assume that the magnitudes shown in Fig. 6a may change by a few millibars (and thus the location of the zero line) when determining the TC impact alone by removing the prestorm large-scale anomalous features in the MPI field. Until this is performed, one cannot conclude that the intensified MPI field 30 days after the TC is due to TC impacts.

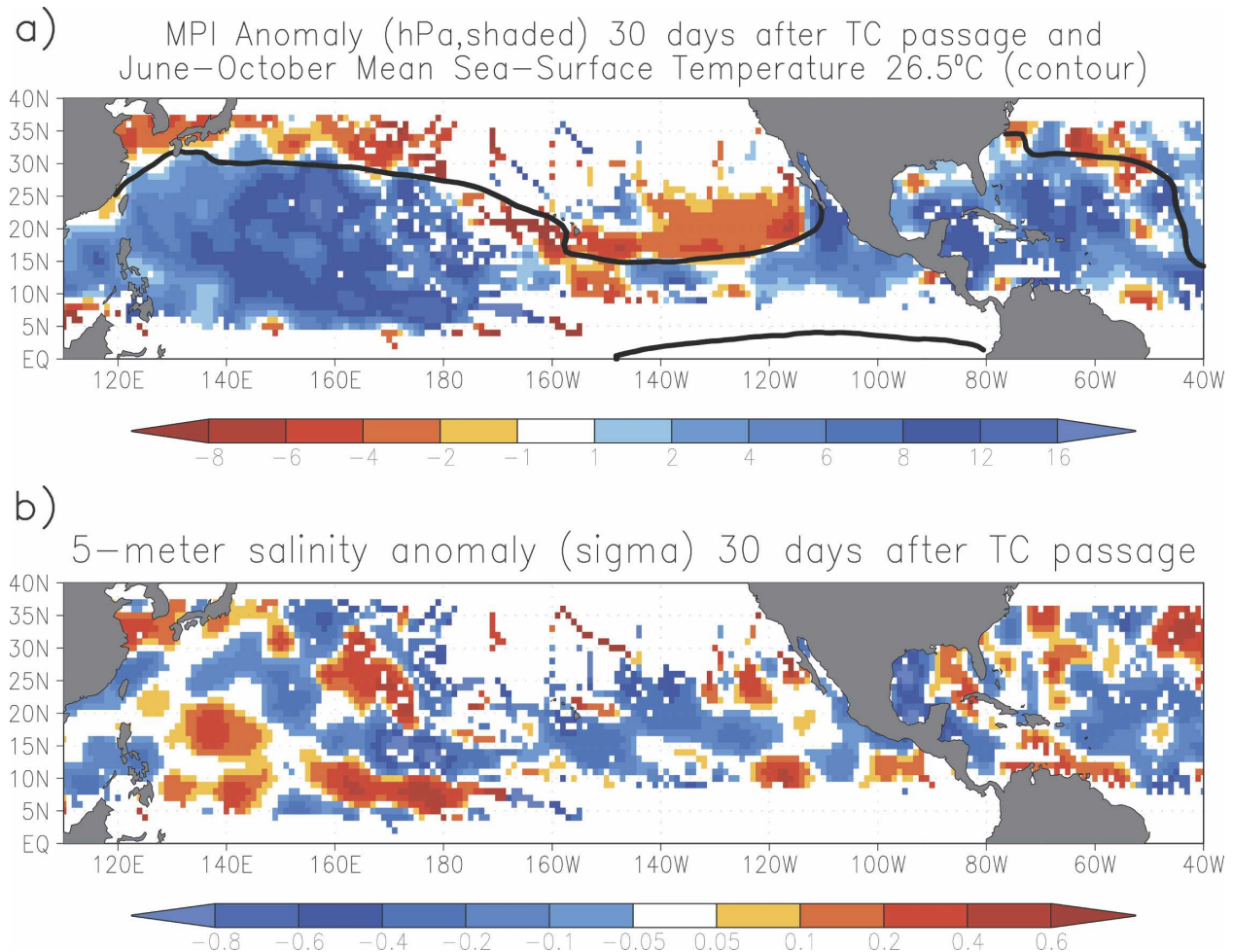


FIG. 10. (a) MPI anomaly (shaded, hPa) 30 days after TC passage, for all TCs of all intensity in the period described in section 2. Negative indicates the MPI is more intense (pressure) than climatology, 30 days after a TC passes that location. This figure was produced by smoothing the native grid ( $1^\circ \times 1^\circ$ ) with a 9-point smoother three times. The black contour is the 26.5°C SST threshold for June–October. (b) Salinity anomaly at 5-m depth 30 days after TC passage, for all TCs of all intensity as described in section 2. Negative indicates the salinity is less than climatology, 30 days after a TC passes that location. This figure was produced by smoothing the native grid ( $1^\circ \times 1^\circ$ ) with a 9-point smoother three times. Source of data for (b): NCEP GODAS (Derber and Rosati 1989; Behringer and Xue 2004).

It is possible that some combination of factors above (or some not yet acknowledged) are combining or negating one another, leading to the localized intensification of MPI 30 days after TC passage.

Finally, it is also worth noting that considerable mesoscale structure exists in Fig. 10a. Of particular interest are those mesoscale regions that are well separated from the strong meridional SST gradient. For example, a circular eddy of enhanced MPI exists over the northwest Gulf of Mexico—in a region that is frequented by TCs. Given the displacement from the Loop Current warm eddy (Shay et al. 2000), it is speculated that TC landfall leads to heavy rainfall over the Mississippi Valley, which is warmed by sensible heat flux and insolation leading to river deposits of a warm freshwater lens

on top of gulf water (Robertson and Ginis 2002). This factor may be further enhanced if prior TC-induced upwelling of cool gulf water might then lead to a more stable oceanic profile over which the low-salinity, warmer river water would then accumulate. Figure 2b (Hurricane Kate, 1985) may illustrate this effect maximized 10 days after passage for a specific case, with the long-term mean impact discussed in section 3e. Further examination is needed to determine this conclusively since continental air mass changes this time of year can also lead to a sudden strengthening of MPI in the Gulf of Mexico after TC passage.

Another mesoscale area of strengthened MPI 30 days after TC passage is just west of Central America. Given that the highest terrain of Central America resides just

northeast of this region, it is possible that the terrain-induced excessive TC rainfall runoff leads to a warm freshwater lens up to 30 days after TC passage in this region. Another possibility is that the TC passage leads to a modification of the gap winds well documented in this region (Xie et al. 2005), which may reduce the normally strong upwelling in this region.

#### *e. Intrabasin variability in salinity changes*

The pattern of upwelling and downwelling associated with the TC wind stresses upon the ocean necessarily results in changes to the salinity of the upper ocean. These changes are in part caused by the oceanic vertical velocity field being imposed upon a nonconstant vertical salinity profile. Additionally, suppression of further precipitation can lead to increased evaporation and an increase in salinity. To quantify these changes, the mean salinity anomaly 30 days after TC passage is calculated (Fig. 10b) for 5-m depth using the NCEP Global Ocean Data Assimilation System (GODAS) dataset (Derber and Rosati 1989). There are coherent patterns of long-lasting significant anomalies in the salinity field, likely dependent in part on whether the ocean is higher or lower salinity beneath the surface and also in part on the static stability of that layer in the presence of upwelling.

There are also interesting mesoscale structures to the salinity anomaly field that partly correlate with Fig. 10a. There is a strong dipole of salinity anomaly in the Gulf of Mexico, with significantly lowered (increased) salinity in the western (eastern) gulf. There is intriguing collocation of the maximum negative salinity anomaly in the western gulf with the warm SST anomaly (Fig. 10a). In this region, there is consistently a warm, freshwater anomaly 30 days after TC passage. This region is generally too far northwest to be explained by the well-documented Loop Current (Shay et al. 2000). Given that most TCs in this region ultimately make landfall in the central or western Gulf Coast, one possible explanation for this collocation is anomalous Mississippi River deposits, as speculated earlier. Moreover, tropical regions adjacent to land have a pronounced tendency toward lowered salinity 30 days after passage (Florida, Mexico, Taiwan), perhaps explained in part by rainfall runoff. Considerable further research is needed to verify or invalidate the preliminary results presented above.

#### **4. Concluding summary**

The analysis of MPI anomaly prior to, during, and following tropical cyclone passage has shown that the tropical atmospheric memory of a TC is approximately one week and the oceanic memory is approximately 1–2

months, depending on storm intensity, lifespan, and basin of occurrence. The removal of atmospheric memory occurs seemingly through radiative cooling of the warmer upper atmosphere to space, rising SLP after TC passage, suppressed convection and latent heat release, and sensible cooling from the underlying upwelled ocean. The removal of oceanic memory is accomplished through temporary heat flux from the atmosphere to the ocean, enhanced insolation resulting from a more stable poststorm sounding, along with (after the peak of the TC season) advancing of the solar calendar and a subsequent weakening of climatological MPI. This oceanic memory removal may also be accelerated in certain regions through low-salinity rainfall accumulation, leading to a suppression of oceanic mixing and accelerated SST warming.

The memory calculated here is for the region over which the TC tracks. What was not directly calculated here is the spatial scale over which the memory extends and how that memory varies temporally away from the TC track itself. Indeed, it follows that the energy utilized to restore the TC track region back to MPI climatology would not necessarily have been utilized for that purpose had the TC never occurred. Thus, the energy budget of the basin and perhaps hemisphere as a whole is altered by the formation of a long-lived and intense TC, presenting a potential feedback that remains largely unquantified but may be hinted at in section 3c. In that regard, the spatial and temporal scale of the memory of a TC may be considerably larger than that calculated here and vary considerably with geography.

These results confirm Emanuel (2001), which suggested that TCs play a critical role in the energy balance of the ocean–atmosphere system. It is apparent from these results that the subtropical and tropical SSTs can easily be a few degrees Celsius warmer or colder than normal at the start of winter simply as a result of anomalous aggregate TC occurrence. Such anomalous SSTs and atmospheric profiles could potentially drive larger-scale atmospheric circulation anomalies and snow cover anomalies into the start of winter, perhaps helping to explain the correlations found in Hart et al. (2007).

#### **5. Discussion and future work**

The memory calculated here directly relates to the frequency of occurrence of tropical cyclones within a given basin. A major tropical cyclone drives a large-scale atmospheric subsidence pattern and an oceanic cooling that suppresses further formation or intensification of TCs on average. Additionally, it was shown that the MPI field itself has a wavelike structure that

varies on the weekly to biweekly scale. When the MPI memory time scale quantified here is combined with the typical translation speed of a TC, the size of a basin, and the period of atmospheric (wave) forcing implied by Fig. 9 and the prior work of Frank and Roundy (2006), it may be possible to begin to explain why there are closer to 100 TCs globally, rather than 10 or 1000.

Future research should further examine the role of tropical cyclones in climate. Mesoscale modeling should extend the work of McTaggart-Cowan et al. (2006) by tracking with higher resolution the forcing introduced by a tropical cyclone that otherwise would not have existed. Climate modeling should examine the changes in overall climate means and variability when tropical cyclones are encouraged (prevented) from forming. It has been argued that trade winds in climate models are too strong, in part, because of the inability of those models to resolve tropical cyclones and the energy transports implied by them (Trenberth and Stepaniak 2003a,b; Trenberth and Fasullo 2007). Such results, when combined with those of Hart et al. (2007) and those shown here, imply that to correctly simulate the global climate for the correct reasons it may be imperative to accurately simulate the intensity and track of tropical cyclones within global climate models.

*Acknowledgments.* This research was funded by NSF Grant ATM-0627908. The second author was supported by a NASA Graduate Fellowship. The third author was partially supported by the Florida State University Department of Meteorology. The authors greatly appreciate critical and constructive input by Mark Bourassa, Carol-Anne Clayson, and Clark Evans of The Florida State University, Jenni Evans of The Pennsylvania State University, Jim Kossin of CIMSS/University of Wisconsin, and two anonymous reviewers. This work would not have been possible without the availability of the ERA-40 dataset provided by ECMWF through NCAR, the SST dataset provided through NASA, and oceanic salinity dataset provided through NCEP and NCAR. The authors are grateful to Kerry Emanuel for providing his MPI subroutine. All figures in this paper were produced using GrADS, provided by COLA/IGES.

#### REFERENCES

- Behringer, D. W., and Y. Xue, 2004: Evaluation of the global ocean data assimilation system at NCEP: The Pacific Ocean. Preprints, *Eighth Symp. on Integrated Observing and Assimilation Systems for Atmosphere, Oceans, and Land Surface*, Seattle, WA, Amer. Meteor. Soc., 2.3.
- Black, P. G., 1983: Ocean temperature change induced by tropical cyclones. Ph.D. dissertation, The Pennsylvania State University, 278 pp. [Available from The Pennsylvania State University, 503 Walker Building, University Park, PA 16802.]
- , and G. J. Holland, 1995: The boundary layer of Tropical Cyclone Kerry (1979). *Mon. Wea. Rev.*, **123**, 2007–2028.
- , R. L. Elsberry, L. K. Shay, R. P. Partridge, and J. D. Hawkins, 1988: Atmospheric boundary layer and oceanic mixed layer observations in Hurricane Josephine obtained from air-deployed drifting buoys and research aircraft. *J. Atmos. Oceanic Technol.*, **5**, 683–698.
- Boos, W. R., J. R. Scott, and K. A. Emanuel, 2004: Transient diapycnal mixing and the meridional overturning circulation. *J. Phys. Oceanogr.*, **34**, 334–341.
- Brewster, J. K., and L. K. Shay, 2006: Oceanic heat content variability in eastern Pacific Ocean. Preprints, *27th Conf. on Hurricanes and Tropical Meteorology*, Monterey, CA, Amer. Meteor. Soc., 6C.3.
- Briegel, L. M., and W. M. Frank, 1997: Large-scale influences on tropical cyclogenesis in the western North Pacific basin. *Mon. Wea. Rev.*, **125**, 1397–1413.
- Burpee, R. W., 1972: The origin and structure of easterly waves in the lower troposphere of North Africa. *J. Atmos. Sci.*, **29**, 77–90.
- Carlson, T. N., and J. M. Prospero, 1972: The large-scale movement of Saharan air outbreaks over the north equatorial Atlantic. *J. Appl. Meteor.*, **11**, 283–297.
- Chu, J.-H., C. R. Sampson, A. S. Levine, and E. Fukada, 2002: The Joint Typhoon Warning Center tropical cyclone best-tracks, 1945–2000. [Available online at [https://metocph.nmci.navy.mil/jtwc/best\\_tracks/](https://metocph.nmci.navy.mil/jtwc/best_tracks/).]
- Derber, J. C., and A. Rosati, 1989: A global oceanic data assimilation system. *J. Phys. Oceanogr.*, **19**, 1333–1347.
- Dickey, T., and Coauthors, 1998: Upper ocean temperature response to Hurricane Felix as measured by the Bermuda test-bed mooring. *Mon. Wea. Rev.*, **126**, 1195–1201.
- Elsberry, R. L., Ed., 1995: Global perspectives on tropical cyclones. WMO Tech. Doc. 693, Geneva, Switzerland, 289 pp.
- , T. Fraim, and R. Trapnell, 1976: A mixed layer model of the ocean thermal response to hurricanes. *J. Geophys. Res.*, **81**, 1153–1162.
- Emanuel, K. A., 1986: An air–sea interaction theory for tropical cyclones. Part I: Steady state maintenance. *J. Atmos. Sci.*, **43**, 585–604.
- , 1988: The maximum intensity of hurricanes. *J. Atmos. Sci.*, **45**, 1143–1155.
- , 2001: The contribution of tropical cyclones to the oceans' meridional heat transport. *J. Geophys. Res.*, **106**, 771–781.
- , 2005: Increasing destructiveness of tropical cyclones over the past 30 years. *Nature*, **436**, 686–688.
- , cited 2006: Subroutine to calculate the maximum wind speed and minimum central pressure achievable in tropical cyclone, given a sounding and sea-surface temperature. [Available online at [ftp://texmex.mit.edu/pub/emanuel/TCMAX/pcmin\\_revised.f](ftp://texmex.mit.edu/pub/emanuel/TCMAX/pcmin_revised.f).]
- Evans, J. L., 1993: Sensitivity of tropical cyclone intensity to sea surface temperature. *J. Climate*, **6**, 1133–1140.
- Ffield, A. F., 2007: Amazon and Orinoco River plumes and NBC rings: Bystanders or participants in hurricane events? *J. Climate*, **20**, 316–333.
- Frank, W. M., 1977: The structure and energetics of the tropical cyclone. I. Storm structure. *Mon. Wea. Rev.*, **105**, 1119–1135.
- , and P. E. Roundy, 2006: The role of tropical waves in tropical cyclogenesis. *Mon. Wea. Rev.*, **134**, 2397–2417.
- , and G. S. Young, 2007: The interannual variability of tropical cyclones. *Mon. Wea. Rev.*, **135**, 3587–3598.

- Gray, W. M., 1985: Tropical cyclone climatology. WMO Tech. Doc. 72, Vol. 1, Geneva, Switzerland, 145 pp.
- Hack, J. J., W. H. Schubert, D. E. Stevens, and H.-C. Kuo, 1989: Response of the Hadley circulation to convective forcing within the ITCZ. *J. Atmos. Sci.*, **46**, 2957–2973.
- Harr, P. A., and R. L. Elsberry, 1995a: Large-scale circulation variability over the tropical western North Pacific. Part I: Spatial patterns and tropical cyclone characteristics. *Mon. Wea. Rev.*, **123**, 1225–1246.
- , and —, 1995b: Large-scale circulation variability over the tropical western North Pacific. Part II: Persistence and transition characteristics. *Mon. Wea. Rev.*, **123**, 1247–1268.
- Hart, R. E., L. F. Bosart, and C. Hosler, 2007: The possible seasonal climate impact from anomalous frequency of recurving tropical cyclones. Preprints, *19th Conf. on Climate Variability and Change*, San Antonio, TX, Amer. Meteor. Soc., 6.3.
- Hong, X., S. Chang, S. Raman, L. K. Shay, and R. Hodur, 2000: The interaction between Hurricane Opal (1995) and a warm core ring in the Gulf of Mexico. *Mon. Wea. Rev.*, **128**, 1347–1365.
- Jarvinen, B. R., C. J. Neumann, and M. A. S. Davis, 1984: A tropical cyclone data tape for the North Atlantic basin, 1886–1983: Contents, limitations, and uses. NOAA Tech. Memo. NWS NHC 22, 21 pp.
- Jacob, S. D., and C. J. Koblinsky, 2007: Effects of precipitation on the upper-ocean response to a hurricane. *Mon. Wea. Rev.*, **135**, 2207–2225.
- Jones, S., C. Velden, S. Aberson, J. Abraham, and P. Harr, 2003: ET, Thorpex, and the North Atlantic TrEC. *Proc. Second Int. Workshop on ET*, Halifax, NS, Canada, Environment Canada, Canadian Hurricane Center, and World Meteorological Organization, P.3.
- Kalnay, E., and Coauthors, 1996: The NCEP/NCAR 40-Year Reanalysis Project. *Bull. Amer. Meteor. Soc.*, **77**, 437–472.
- Karyampudi, V. M., and H. F. Pierce, 2002: Synoptic-scale influence of the Saharan air layer on tropical cyclogenesis over the eastern Atlantic. *Mon. Wea. Rev.*, **130**, 3100–3128.
- Kelsey, E. P., and L. F. Bosart, 2006: Supertyphoon Dale (1996): A remarkable storm from birth through extratropical transition to explosive reintensification that impacted the tropics, midlatitudes, and Arctic. Preprints, *27th Conf. on Hurricanes and Tropical Meteorology*, Monterey, CA, Amer. Meteor. Soc., 3A.4.
- Landsea, C. W., B. A. Harper, K. Hoarau, and J. Knaff, 2006: Can we detect trends in extreme tropical cyclones? *Science*, **313**, 452–454.
- Leipper, D., 1967: Observed ocean conditions and Hurricane Hilda, 1964. *J. Atmos. Sci.*, **24**, 182–196.
- Manning, D., and R. E. Hart, 2007: Evolution of North Atlantic ERA40 tropical cyclone representation. *Geophys. Res. Lett.*, **34**, L05705, doi:10.1029/2006GL028266.
- Mao, Q., S. W. Chang, and R. L. Pfeffer, 2000: Influence of large-scale initial oceanic mixed layer depth on tropical cyclones. *Mon. Wea. Rev.*, **128**, 4058–4070.
- McTaggart-Cowan, R., L. F. Bosart, J. R. Gyakum, and E. Atallah, 2006: Evolution and global impacts of a diabatically-generated warm pool: Hurricane Katrina (2005). Preprints, *27th Conf. on Hurricanes and Tropical Meteorology*, Monterey, CA, Amer. Meteor. Soc., 4A.8.
- Neumann, C. J., B. R. Jarvinen, C. J. McAdie, and J. D. Elms, 1993: Tropical cyclones of the North Atlantic Ocean, 1871–1992. National Climatic Data Center in cooperation with the National Hurricane Center, Coral Gables, FL, 193 pp. [The most recent track information is available online at <http://www.nhc.noaa.gov/>]
- Newton, C. W., Eds., 1972: *Meteorology in the Southern Hemisphere. Meteor. Monogr.*, No. 35, Amer. Meteor. Soc., 263 pp.
- Price, J. F., 1981: Upper ocean response to a hurricane. *J. Phys. Oceanogr.*, **11**, 153–175.
- Ramanathan, V., and W. Collins, 1991: Thermodynamic regulation of ocean warming by cirrus clouds deduced from observations of the 1987 El Nino. *Nature*, **351**, 27–32.
- Reynolds, R. W., K. S. Casey, T. M. Smith, and D. B. Chelton, 2006: A daily blended analysis for sea surface temperature. Preprints, *14th Conf. on Satellite Meteorology and Oceanography*, Atlanta, GA, Amer. Meteor. Soc., 8.1.
- Robertson, E. J., and I. Ginis, 2002: The upper ocean salinity response to tropical cyclones. Preprints, *25th Conf. on Hurricanes and Tropical Meteorology*, San Diego, CA, Amer. Meteor. Soc., 14D.5.
- Roundy, P. E., and W. M. Frank, 2004: A climatology of waves in the equatorial region. *J. Atmos. Sci.*, **61**, 2105–2132.
- Schubert, W. H., P. E. Ciesielski, D. E. Stevens, and H. C. Kuo, 1991: Potential vorticity modeling of the ITCZ and the Hadley circulation. *J. Atmos. Sci.*, **48**, 1493–1509.
- Shay, L. K., R. L. Elsberry, and P. G. Black, 1989: Vertical structure of the ocean current response to a hurricane. *J. Phys. Oceanogr.*, **19**, 649–669.
- , G. J. Goni, and P. G. Black, 2000: Effects of a warm oceanic feature on Hurricane Opal. *Mon. Wea. Rev.*, **128**, 1366–1383.
- Sobel, A. H., and S. J. Camargo, 2005: Influence of western Pacific tropical cyclones on their large-scale environment. *J. Atmos. Sci.*, **62**, 3396–3407.
- Subrahmanyam, B., V. S. N. Murty, R. J. Sharp, and J. J. O'Brien, 2005: Air-sea coupling during the tropical cyclones in the Indian Ocean: A case study using satellite observations. *Pure Appl. Geophys.*, **162**, 1643–1672.
- Trenberth, K. E., and D. Stepaniak, 2003a: Covariability of components of poleward atmospheric energy transports on seasonal and interannual timescales. *J. Climate*, **16**, 3691–3705.
- , and —, 2003b: Seamless poleward atmospheric energy transports and implications for the Hadley circulation. *J. Climate*, **16**, 3706–3722.
- , and J. Fasullo, 2007: The water and energy budgets of hurricanes and implications for climate change. Preprints, *AMS Forum: Climate Change Manifested by Changes in Weather*, San Antonio, TX, Amer. Meteor. Soc., 1.9.
- Uppala, S. M., and Coauthors, 2005: The ERA-40 reanalysis. *Quart. J. Roy. Meteor. Soc.*, **131**, 2961–3012.
- Watson, M., 2005: A recalculation of MPI using upper-ocean depth-averaged temperatures: Climatology and case studies. M.S. thesis, Dept. of Meteorology, The Florida State University, 112 pp. [Available online at <http://etd.lib.fsu.edu/theses/available/etd-07122005-133321/>.]
- Webster, P. J., G. J. Holland, J. A. Curry, and H.-R. Chang, 2005: Changes in tropical cyclone number, duration, and intensity in a warming environment. *Science*, **309**, 1844–1846.
- Wheeler, M., and G. Kiladis, 1999: Convectively coupled equatorial waves: Analysis of clouds and temperature in the wave-number–frequency domain. *J. Atmos. Sci.*, **56**, 374–399.
- Xie, S.-P., H. Xu, W. S. Kessler, and M. Nonaka, 2005: Air–sea interaction over the eastern Pacific warm pool: Gap winds, thermocline dome, and atmospheric convection. *J. Climate*, **18**, 5–20.